

Kinetic and Diffusion Driven Instabilities in the Bromate-Sulfite-Ferrocyanide System

István Molnár^{†,‡} and István Szalai^{*,†}

[†]*Institute of Chemistry, Eötvös University, Budapest, Hungary*

[‡]*School of Ph.D. Studies, Semmelweis University, Budapest, Hungary*

E-mail: szalai.istvan@chem.elte.hu

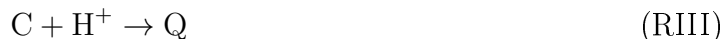
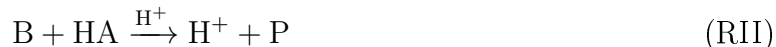
Abstract

The spatiotemporal dynamics of the Bromate-Sulfite-Ferrocyanide (BSF) reaction-diffusion system in a open one-side-fed reactor (OSFR) is investigated by numerical simulations. The results of the simulations are compared with experiments performed in an annular shape OSFR. Both kinetic and diffusion driven instabilities are identified in the model. There are two hydrogen ion consuming pathways in the mechanism, the partial oxidation of sulfite to dithionate and the oxidation of ferrocyanide by bromate ions. The dynamical effects of them are similar as they support the same negative feedback loop via sulfite ion. However, the time scale of the oxidation of ferrocyanide by bromate ions can be conveniently controlled by the input feed concentrations, thus it provides a more flexible way find spatiotemporal oscillations. Long range activation due to the relative fast diffusion of hydrogen ions compared to the other reactants can also result in oscillations in this mechanism. We show, that the spatial extent of the reaction-diffusion medium along the direction of the diffusive feed (the thickness) acts as a general control parameter of the dynamics. Oscillations, either originated in kinetic or in diffusive instabilities, can only develop in a narrow range of the thickness. This property explains the experimentally often observed spatial localization of the oscillations. A reciprocal relationship is found between two main control parameters of the dynamics, which are the thickness and the hydrogen ion input feed concentration.

Introduction

Pattern formation is often the result of time and length scale separation of the feedbacks, which drive chemical or biochemical processes. One of the most studied chemical examples of temporal and spatiotemporal self-organization are the mixed Landolt type reactions.^{1,2} These systems are capable to show bistability and oscillations in a continuous-flow stirred tank reactors (CSTR),¹ chemical waves and stationary patterns in an open one-side-fed reactor (OSFR),³⁻⁸ and also to drive periodic volume changes of hydrogels.⁹⁻¹³ A general

skeleton mechanism of the mixed Landolt systems consists of three reaction steps (RI-RIII).¹⁴



It is based on the acid catalyzed oxidation of a weak acid (HA) by an oxidant (B) in reaction (RII), supplemented with a proton consuming reaction (RIII) induced by component C. Here, P and Q are end products. In the experiments, sulfite ions are most often used as component A^- whereas the typical oxidant is iodate, bromate, or hydrogen peroxide. The proton consuming reaction (RIII) can be actualized by the reaction between the oxidant (B) and ferrocyanide, thiosulfate or thiourea, or by using the protonation equilibrium of hydrogen-carbonate.¹ This large variety of chemistry provides a necessary flexibility for the experimental realization of a wide range of dynamical behavior.

Reaction-diffusion phenomena can develop due to kinetic and diffusion driven instabilities in mixed Landolt systems in an OSFR. In this type of reactors all space points are maintained at appropriate distance from thermodynamic equilibrium by the input of fresh chemical and withdrawal of end products. An OSFR consists in a piece of porous material set in contact with the contents of a CSTR. Typically, the porous material is a chemically inert hydrogel. The transport of chemical species inside the gel and the exchanges of matter between the gel and its environment is provided by diffusion. The gel medium avoids any hydrodynamic flow, thus pure reaction-diffusion behavior can develop inside it. The usual operation mode of an OSFR is, when the mixture of the CSTR is kept on a low extent of reaction state, thus the gel is fed by fresh reactants. An OSFR (Figure 1a) can be described by the next set of

equations:

$$\begin{aligned} \frac{d\mathbf{c}_{\text{cstr}}}{dt} = & \mathbf{f}(\mathbf{c}_{\text{cstr}}, k_1, k_2 \dots k_n) + k_0(\mathbf{c}_0 - \mathbf{c}_{\text{cstr}}) \\ & + \rho_V \frac{\mathbf{D}}{L_x} \left[\frac{\partial \mathbf{c}}{\partial x} \right]_{x=0} \end{aligned} \quad (1)$$

and

$$\partial_t \mathbf{c} = \mathbf{f}(\mathbf{c}, k_1, k_2 \dots k_n) + \mathbf{D} \Delta \mathbf{c} \quad (2)$$

Dirichlet b. c. at $x = 0 (\forall y, z) : \mathbf{c}(x = 0, y, z) = \mathbf{c}_{\text{cstr}}$

No-flux boundary condition at all other gel surfaces

where \mathbf{c}_{cstr} are the concentrations in the CSTR, \mathbf{f} describe the kinetic functions of each species, k_1, k_2, \dots, k_n are the rate constants, k_0 is the reciprocal residence time of the CSTR, \mathbf{c}_0 are the concentrations in the input flow of the CSTR, \mathbf{D} is the diagonal matrix of the diffusion coefficients, L_x is the size of the gel in the x -direction, ρ_V is the ratio between the volume of the gel and that of the CSTR and \mathbf{c} are the concentrations in the gel. The last term of equation (1) can generally be neglected if $\rho_V \ll 1$. The concentrations in the CSTR fix the boundary feed composition at the CSTR/gel interface. The mixed boundary conditions have significant effects on the reaction-diffusion dynamics observed in these type of reactors.

Reaction systems exhibiting bistability in a CSTR, like the Landolt type reactions, can lead to a phenomenon called “spatial bistability” when they are operated in an OSFR.^{15–17} This phenomenon corresponds to the coexistence of two different concentration profiles in the gel along the direction (here it is denoted with x) of the diffusive feed, for the same fixed composition of the CSTR contents. For continuity reason, the composition in the gel nearby the gel/CSTR boundary ($x = 0$) must be similar to that of the CSTR. Here, we study the dynamics in the gel, when the CSTR is kept on a low extent of reaction stationary

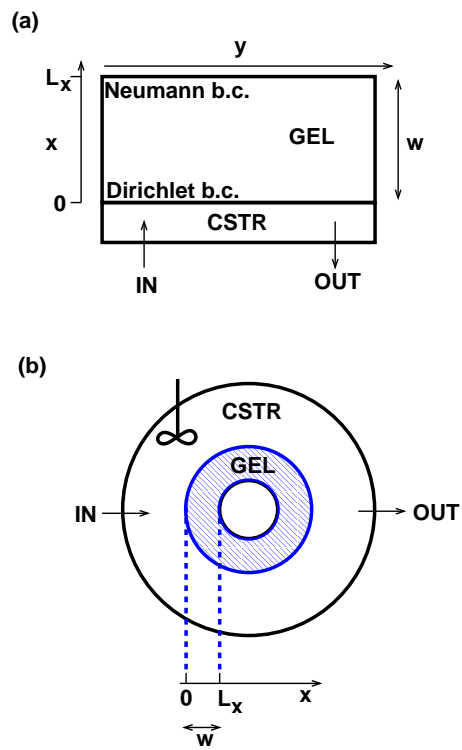


Figure 1: Geometry of an open one-side-fed gel reactor (OSFR) used in the simulations (a), and the sketch of an annular OSFR applied in the experiments. Here w denotes the thickness of the gel along the x direction. The extent of the gel along the third dimension (z) is neglected here. The volume of the CSTR is much larger than that of the gel.

state. Now, the composition inside the gel along the x direction depends on the actual time scale of the the diffusive feed and that of the reaction. When the time scale of the diffusive feed at each space points along x is shorter than that of the reaction, the extent of reaction remains low in the whole gel. This state is called as the F “flow” state of the gel. At the other spatial state the time scale of the diffusive feed in the depth of the gel, e.g. at $x = L_x$, is longer than the time scale of the reaction, thus the extent of reaction becomes high in the inner part of the gel. But, a boundary layer at the gel/CSTR interface remains in the low extent of reaction state, as we have discussed. This second spatial state is characterized by a relatively sharp chemical front between the unreacted and the reacted states and called as M “mixed” state of the gel. It has been shown theoretically by using a general cubic autocatalytic model, that the appearance of spatial bistability is the consequence of the Dirichlet boundary condition at the gel/CSTR surface and the finite thickness of the gel.¹⁶

The presence of an additional hydrogen ion consuming reaction, can induce spatiotemporal oscillations in mixed Landolt reactions operated in an OSFR, by using either iodate, bromate or hydrogen peroxide as an oxidant.^{3-6,8} The theoretical conditions for the development of oscillations due to a kinetic instability in an OSFR are not known, but numerical simulations with a model consists of reactions (RI-RIII) are ready to account the basic aspects of the dynamics.² The performance of this skeleton model is naturally limited. For example, in parallel to the pH patterns triiodide patterns also form in the iodate-sulfite-ferrocyanide (FIS) reaction,¹⁸ but this behavior have not observed in the analogous iodate-sulfite-thiourea (TuIS) reaction. As interesting phenomenon is the formation of the peculiar filamentous network structure, that was detected in the hydrogen-peroxide-sulfite-hydrogen carbonate (HPSC) reaction,⁵ which has only some reminiscence in the FIS system. The explanation of these behaviors would require the use of realistic chemical models in numerical simulations.

In an OSFR, due to the diffusive matter exchange between the CSTR content and the gel, a diffusion driven instability can also results in the development of spatiotemporal oscil-

lations. This has been experimentally first observed in the chlorite-tetrathionate reaction.¹⁹ The theoretical study of this bifurcation has shown that the oscillations emerge from a Hopf bifurcation when the diffusion coefficient of the autocatalyst is larger than that of the other reactants (long-range activation).¹⁵ This prerequisite is naturally fulfilled in the mixed Landolt type reactions, since hydrogen ions diffuses much faster than the other components. Numerical simulations with the skeleton model consists of reactions (RI-RII) are ready to show long range activation oscillations.²⁰ But, this is not supported by the experiments. Until now, this phenomenon have been observed experimentally only in the iodate-sulfite (IS) reaction,²¹ and not in the bromate-sulfite (BS) or in the hydrogen peroxide-sulfite (HPS) reactions.^{5,22} The reason for the different behaviors of the analogous systems has not been clarified yet. The reported numerical simulations with detailed model of the IS reaction show long-range activation,²² and only kinetic instabilities driven oscillations found in the model of the BS reaction.²³

Here, we present a numerical study of the bromate-sulfite-ferrocyanide (BSF) reaction-diffusion system, supplemented with experiments made in an annular OSFR. The model we used in the simulations (Table 1) is based on the work of Rábai and coworkers.^{24,25} The complex mechanism of the oxidation of ferrocyanide by bromate ions is²⁶ described by a simplified way with reactions (R6 and R7) following the suggestion of Epstein and coworkers.²⁷

Table 1: Kinetic model used in numerical simulations

	reactions	rate laws
R1	$\text{SO}_3^{2-} + \text{H}^+ \rightleftharpoons \text{HSO}_3^-$	$r_1 = k_1[\text{SO}_3^{2-}][\text{H}^+] - k_{-1}[\text{HSO}_3^-]$
R2	$\text{HSO}_3^- + \text{H}^+ \rightleftharpoons \text{H}_2\text{SO}_3$	$r_2 = k_2[\text{HSO}_3^-][\text{H}^+] - k_{-2}[\text{H}_2\text{SO}_3]$
R3	$\text{BrO}_3^- + 3\text{HSO}_3^- \rightarrow 3\text{SO}_4^{2-} + \text{Br}^- + 3\text{H}^+$	$r_3 = k_3[\text{HSO}_3^-][\text{BrO}_3^-]$
R4	$\text{BrO}_3^- + 3\text{H}_2\text{SO}_3 \rightarrow 3\text{SO}_4^{2-} + \text{Br}^- + 6\text{H}^+$	$r_4 = k_4[\text{H}_2\text{SO}_3][\text{BrO}_3^-]$
R5	$\text{BrO}_3^- + 6\text{H}_2\text{SO}_3 \rightarrow 3\text{S}_2\text{O}_6^{2-} + \text{Br}^- + 6\text{H}^+ + 3\text{H}_2\text{O}$	$r_5 = k_5[\text{H}_2\text{SO}_3][\text{BrO}_3^-]$
R6	$[\text{Fe}(\text{CN})_6]^{4-} + \text{H}^+ \rightleftharpoons \text{H}[\text{Fe}(\text{CN})_6]^{3-}$	$r_6 = k_6[\text{Fe}(\text{CN})_6^{4-}][\text{H}^+] - k_{-6}[\text{HFe}(\text{CN})_6^{3-}]$
R7	$\text{BrO}_3^- + 6\text{H}[\text{Fe}(\text{CN})_6]^{3-} \rightarrow \text{Br}^- + 6[\text{Fe}(\text{CN})_6]^{3-} + 3\text{H}_2\text{O}$	$r_7 = k_7[\text{HFe}(\text{CN})_6^{3-}][\text{BrO}_3^-]$
R8	$\text{SO}_4^{2-} + \text{H}^+ \rightleftharpoons \text{HSO}_4^-$	$r_8 = k_8[\text{SO}_4^{2-}][\text{H}^+] - k_{-8}[\text{HSO}_4^-]$
R9	$\text{H}^+ + \text{OH}^- \rightleftharpoons \text{H}_2\text{O}$	$r_9 = k_9[\text{H}^+][\text{OH}^-] - k_{-9}$

The BSF reaction is known to show bistability and large amplitude pH-oscillations in a

CSTR.²⁸ In an OSFR diverse spatiotemporal dynamics, including spatial bistability, waves and stationary patterns have been reported in this reaction.^{7,8} The dynamics of the BSF reaction is driven by a positive feedback appear in the oxidation of hydrogen sulfite and sulfurous acid by bromate ions (R3 and R4). This pathway produces hydrogen ions in a autocatalytic manner. This positive feedback is responsible for the bistability phenomena in CSTR and also for spatial bistability in OSFR. The formation of oscillations requires the presence of a negative feedback, e.g. a hydrogen ions consuming process. This is the role of the ferrocyanide, due to its oxidation by bromate ions (R6 and R7). It has been suggested, that beside sulfate ions, dithonate ions can also form in the the oxidation of sulfite bromate ions.^{25,29} This is a sign of an alternative hydrogen ion consuming pathway (R5). Accordingly, temporal or spatiotemporal oscillations can also develop even in the absence of ferrocyanide, in the core BS system.^{22,25} The mechanism presented in Table 1 has been successfully applied to simulate the CSTR dynamics of the BSF reaction,^{24,25} and also some aspects of the OSFR dynamics of the BS reaction.²²

The aim of this paper is to clarify the role of the different feedback mechanisms in the spatiotemporal dynamics of the BSF system operated in an OSFR. This would give some insight into the pattern formation mechanism of the BSF and the analogous Landolt type systems. We also want to find the reason of lack of long-range activation oscillations, which is in principle a general phenomena in hydrogen ion autocatalytic systems, but have not found in the BS reaction.

Experimental and Numerical Methods

The experiments were performed in a thermostatted annular-shape OSFR,³⁰ where the flat annular shape gel was made of 2 w/w% agarose (Fluka 05077) with a thickness $w = 1$ mm and outer diameter 25 mm. All of the faces of the annulus are tightly pressed against impermeable walls, except for the outer edge, which is in direct contact with the contents of a

CSTR. This design makes it possible to observe the color changes across the 1.00 mm width of the flat annulus (Figure 1b). The observations, in reflected light, are made in a direction orthogonal to the direction feed, along the x, y plane. The residence time in the CSTR was fixed to 500 s. The experiments were made at $T=30^\circ\text{C}$. The feed solutions of the major chemicals were stored in four separated tanks but enter premixed into the CSTR. Reactants were distributed in the feed tanks as follows:

Tank 1: NaBrO_3 (Sigma-Aldrich)+ sodium bromocresol green (Sigma-Aldrich); Tank 2: Na_2SO_3 (Sigma-Aldrich) + sodium bromocresol green (Sigma-Aldrich); Tank 3: $\text{K}_4\text{Fe}(\text{CN})_6 \cdot 3\text{H}_2\text{O}$ (Sigma-Aldrich); Tank 4: H_2SO_4 (diluted from 1.0 mol/L standard solution (Sigma-Aldrich)). All solutions were prepared with ion exchanged water and chemicals were used without further purification. The following input feed concentrations were kept fixed in all the experiments: $[\text{NaBrO}_3]_0 = 65\text{ mM}$, $[\text{sodium bromocresol green}]_0 = 0.2\text{ mM}$. Here, $[X]_0$ denotes the concentration that species X would have after mixing in the total inlet flow and prior to any reaction. To visualize the pH patterns bromocresol green indicator ($pK_a = 4.8$) was selected and the reactor was illuminated through a narrow band-pass filter centered at $\lambda = 590 \pm 5\text{ nm}$. The pictures were taken by using a AVT Stingray F-033B (656×492 , 14 bit) camera and recorded by the Streampix (Norpix) software. The image processing are made by using ImageJ. The observed gray scale pictures were colorized to mimic the color change of the applied indicator. The state of the CSTR composition was monitored by the recording the potential of a bright platinum electrode.

The partial differential equations were discretized with a standard second-order finite difference scheme on a 200 mesh in the 1D case (simulations along the x axis), and on a 100×250 mesh in the 2D case. The resulting systems were solved by the SUNDIALS CVODE³¹ solver using the backward differentiation formula method. The absolute and the relative error tolerance were 10^{-15} and 10^{-7} , respectively. The chemistry of model of the BSF reaction is shown in Table 1. For the numerical simulation of the dynamics in an OSFR we used the the following set of equations. The CSTR content is described by the next

equations:

$$\frac{d[\text{H}^+]_{\text{cstr}}}{dt} = -r_1 - r_2 + 3r_3 + 6r_4 + 6r_5 - r_6 - r_8 - r_9 + k_0([\text{H}^+]_0 - [\text{H}^+]_{\text{cstr}}) \quad (3)$$

$$\frac{d[\text{SO}_3^{2-}]_{\text{cstr}}}{dt} = -r_1 + k_0([\text{SO}_3^{2-}]_0 - [\text{SO}_3^{2-}]_{\text{cstr}}) \quad (4)$$

$$\frac{d[\text{HSO}_3^-]_{\text{cstr}}}{dt} = r_1 - r_2 - 3r_3 + k_0([\text{HSO}_3^-]_0 - [\text{HSO}_3^-]_{\text{cstr}}) \quad (5)$$

$$\frac{d[\text{H}_2\text{SO}_3]_{\text{cstr}}}{dt} = r_2 - 3r_4 - 6r_5 + k_0([\text{H}_2\text{SO}_3]_0 - [\text{H}_2\text{SO}_3]_{\text{cstr}}) \quad (6)$$

$$\frac{d[\text{BrO}_3^-]_{\text{cstr}}}{dt} = -r_3 - r_4 - r_5 - r_7 + k_0([\text{BrO}_3^-]_0 - [\text{BrO}_3^-]_{\text{cstr}}) \quad (7)$$

$$\frac{d[\text{Fe}(\text{CN})_6^{4-}]_{\text{cstr}}}{dt} = -r_6 + k_0([\text{Fe}(\text{CN})_6^{4-}]_0 - [\text{Fe}(\text{CN})_6^{4-}]_{\text{cstr}}) \quad (8)$$

$$\frac{d[\text{HFe}(\text{CN})_6^{3-}]_{\text{cstr}}}{dt} = r_6 - 6r_7 + k_0([\text{HFe}(\text{CN})_6^{3-}]_0 - [\text{HFe}(\text{CN})_6^{3-}]_{\text{cstr}}) \quad (9)$$

$$\frac{d[\text{SO}_4^{2-}]_{\text{cstr}}}{dt} = 3r_3 + 3r_4 - r_8 + k_0([\text{SO}_4^{2-}]_0 - [\text{SO}_4^{2-}]_{\text{cstr}}) \quad (10)$$

$$\frac{d[\text{HSO}_4^-]_{\text{cstr}}}{dt} = r_8 + k_0([\text{HSO}_4^-]_0 - [\text{HSO}_4^-]_{\text{cstr}}) \quad (11)$$

$$\frac{d[\text{OH}^-]_{\text{cstr}}}{dt} = -r_9 + k_0([\text{OH}^-]_0 - [\text{OH}^-]_{\text{cstr}}) \quad (12)$$

where, $[]_{\text{cstr}}$ and $[]_0$ are concentrations in the CSTR and in the input feed, respectively. The feedback of the gel content on the state of the CSTR is neglected, since in the typical experiment the volume of the CSTR is much larger than that of the gel. All the input feed concentrations are set to be zero, except $[\text{H}^+]_0$, $[\text{SO}_3^{2-}]_0$, $[\text{BrO}_3^-]_0$ and $[\text{Fe}(\text{CN})_6^{4-}]_0$. The

reaction-diffusion system is described by the following equations:

$$\partial_t[\text{H}^+] = -r_1 - r_2 + 3r_3 + 6r_4 + 6r_5 - r_6 - r_8 - r_9 + D_{\text{H}^+}\Delta[\text{H}^+] \quad (13)$$

$$\partial_t[\text{SO}_3^{2-}] = -r_1 + D_{\text{SO}_3^{2-}}\Delta[\text{SO}_3^{2-}] \quad (14)$$

$$\partial_t[\text{HSO}_3^-] = r_1 - r_2 - 3r_3 + D_{\text{HSO}_3^-}\Delta[\text{HSO}_3^-] \quad (15)$$

$$\partial_t[\text{H}_2\text{SO}_3] = r_2 - 3r_4 - 6r_5 + D_{\text{H}_2\text{SO}_3}\Delta[\text{H}_2\text{SO}_3] \quad (16)$$

$$\partial_t[\text{BrO}_3^-] = -r_3 - r_4 - r_5 - r_7 + D_{\text{BrO}_3^-}\Delta[\text{BrO}_3^-] \quad (17)$$

$$\partial_t[\text{Fe}(\text{CN})_6^{4-}] = -r_6 + D_{\text{Fe}(\text{CN})_6^{4-}}\Delta[\text{Fe}(\text{CN})_6^{4-}] \quad (18)$$

$$\partial_t[\text{HFe}(\text{CN})_6^{3-}] = r_6 - 6r_7 + D_{\text{HFe}(\text{CN})_6^{3-}}\Delta[\text{HFe}(\text{CN})_6^{3-}] \quad (19)$$

$$\partial_t[\text{SO}_4^{2-}] = 3r_3 + 3r_4 - r_8 + D_{\text{SO}_4^{2-}}\Delta[\text{SO}_4^{2-}] \quad (20)$$

$$\partial_t[\text{HSO}_4^-] = r_8 + D_{\text{HSO}_4^-}\Delta[\text{HSO}_4^-] \quad (21)$$

$$\partial_t[\text{OH}^-] = -r_9 + D_{\text{OH}^-}\Delta[\text{OH}^-] \quad (22)$$

with Dirichlet boundary conditions at the gel/CSTR surface, e.g. $[\text{H}^+]_{(x=0)} = [\text{H}^+]_{\text{cstr}}$, and no flux boundary conditions at the gel/impermeable wall surfaces, e.g. $(\partial_x[\text{H}^+])_{(x=L_x)} = 0$. The rate constants^{22,25,27} and the diffusion coefficients^{22,32} used in the simulations were taken from the literature and listed in Table 2. Here, we assume that the diffusion coefficients of the

Table 2: Rate constants and diffusion coefficients used in the simulations

$k_1 = 5 \times 10^{10} \text{ M}^{-1}\text{s}^{-1}$	$k_{-1} = 3 \times 10^3 \text{ s}^{-1}$
$k_2 = 2 \times 10^8 \text{ M}^{-1}\text{s}^{-1}$	$k_{-2} = 3.4 \times 10^6 \text{ s}^{-1}$
$k_3 = 3.3 \times 10^2 \text{ M}^{-1}\text{s}^{-1}$	
$k_4 = 22 \text{ M}^{-1}\text{s}^{-1}$	
$k_5 = 0.7 \text{ M}^{-1}\text{s}^{-1}$	
$k_6 = 1 \times 10^{10} \text{ M}^{-1} \text{ s}^{-1}$	$k_{-6} = 6 \times 10^6 \text{ s}^{-1}$
$k_7 = 0.085 \text{ M}^{-1}\text{s}^{-1}$	
$k_8 = 1 \times 10^{11} \text{ M}^{-1}\text{s}^{-1}$	$k_{-8} = 1.148 \times 10^3 \text{ s}^{-1}$
$k_9 = 1.4 \times 10^{11} \text{ M}^{-1}\text{s}^{-1}$	$k_{-9} = 1.4 \times 10^{-3} \text{ Ms}^{-1}$
$k_0 = 2 \times 10^{-3} \text{ s}^{-1}$	
$D_{\text{H}^+} = 9.0 \times 10^{-5} \text{ cm}^2\text{s}^{-1}$	$D_{\text{SO}_3^{2-}} = 1.1 \times 10^{-5} \text{ cm}^2\text{s}^{-1}$
$D_{\text{HSO}_3^-} = 1.5 \times 10^{-5} \text{ cm}^2\text{s}^{-1}$	$D_{\text{BrO}_3^-} = 1.485 \times 10^{-5} \text{ cm}^2\text{s}^{-1}$
$D_{\text{Fe}(\text{CN})_6^{4-}} = 0.735 \times 10^{-5} \text{ cm}^2\text{s}^{-1}$	$D_{\text{HFe}(\text{CN})_6^{3-}} = 0.9 \times 10^{-5} \text{ cm}^2\text{s}^{-1}$
$D_{\text{H}_2\text{SO}_3} = 1.6 \times 10^{-5} \text{ cm}^2\text{s}^{-1}$	$D_{\text{SO}_4^{2-}} = 1.065 \times 10^{-5} \text{ cm}^2\text{s}^{-1}$
$D_{\text{HSO}_4^-} = 1.33 \times 10^{-5} \text{ cm}^2\text{s}^{-1}$	$D_{\text{OH}^-} = 5.26 \times 10^{-5} \text{ cm}^2\text{s}^{-1}$

components of the BSF reaction in 2 w/w% agarose gel is the same like in an aqueous solution. Ouyang and coworkers measured the diffusion coefficient of NaCl as a function of the agarose gel density.³³ According to their results in a 2 w/w% agarose gel the diffusion coefficient of NaCl is $1.5 \times 10^{-5} \text{ cm}^2\text{s}^{-1}$ compared to its value in water, that is $1.8 \times 10^{-5} \text{ cm}^2\text{s}^{-1}$. This relatively small difference supports the validity of our assumption. However, the diffusion of hydrogen ions in the agarose gel can be affected by the traces of agarpectin. By considering the typical amount of agarpectin in the applied agarose, this effect can be also neglected.⁵

Experimental Results

A quite reach spatiotemporal dynamics have already been reported when the BSF reaction is performed in an OSFR.^{7,8} The previous experiments were made in a disk shape OSFR, where the quasi 2D patterns are recorded along the (y, z) plane in perpendicular the direction of the diffusive feed (x) . The recorded pictures provides information on the integrated light absorption patterns across the thickness of the disk of gel but not on how the patterns organize within the thickness (e.g. along the (x, y) plane). This informations can be collected by the experiments made in an annular OSFR.

At the conditions used here, in the absence of ferrocyanide or below $[\text{Fe}(\text{CN})_6^{4-}]_0=15 \text{ mM}$, two different spatial states can develop in the gel. At the F state of the OSFR, the gel is in a quasi uniform dark color state. In the pictures, the dark and light gray colors correspond, respectively, to high ($\text{pH} > 4.8$) and low pH ($\text{pH} < 4.8$) compositions in gel. In this case the extent of the reaction is low at each space point in the gel. At M state of the OSFR, the a stable pH-indicator color switch settles parallel to the rim of the annulus. That means the the extent of the reaction is high in the inner part of the gel, and low in the outer part of it. In the parameter domain of spatial bistability, these two states coexist and a perturbation can results in the formation of a moving front, as it is shown in Figure 2. The direction of the propagation of these fronts depends on the actual value of $[\text{H}_2\text{SO}_4]_0$.

The extent of the parameter domain of spatial bistability decreases as $[\text{Fe}(\text{CN})_6^{4-}]_0$ is

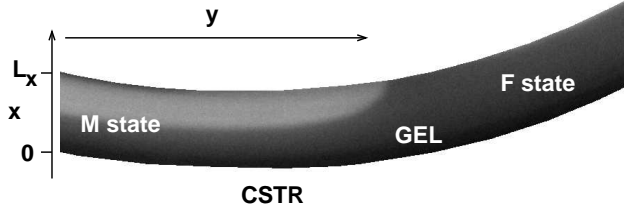


Figure 2: Propagating front in the BSF reaction in the annular OSFR. At the actual conditions the M state domain increases at the expense of the F one in the gel. Experimental conditions: $[\text{BrO}_3^-]_0=65\text{ mM}$, $[\text{SO}_3^{2-}]_0=80\text{ mM}$, $[\text{Fe}(\text{CN})_6^{4-}]_0=5\text{ mM}$, $[\text{H}_2\text{SO}_4]_0=5.0\text{ mM}$ and $w=1.0\text{ mm}$.

increased and vanishes at a critical value $[\text{Fe}(\text{CN})_6^{4-}]_0 \approx 15\text{ mM}$, as it has been reported previously.⁸ Above this limit, in a range of $[\text{H}_2\text{SO}_4]_0$, the innermost part of the gel suddenly become acidic, and the extent of this acidic region moves back and forth across the width of the annulus. In Figure 3a a snapshot of the gel is presented at this oscillatory state, where an

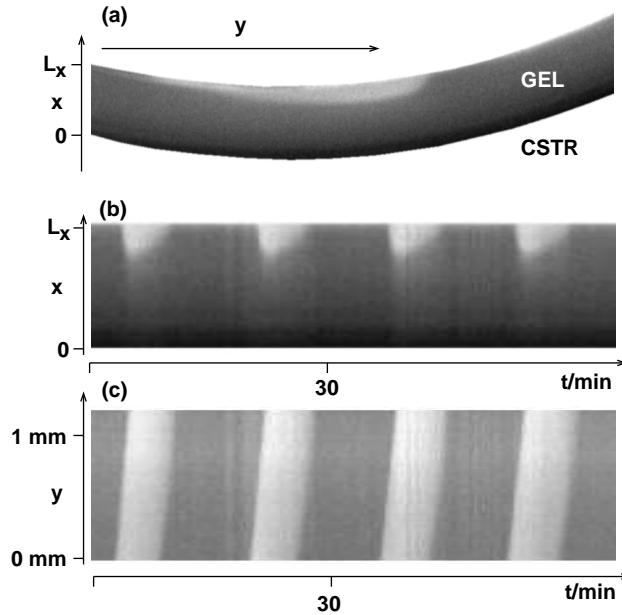


Figure 3: Spatiotemporal oscillations in the BSF reaction in the gel of the annular OSFR (a), and the corresponding time-space plots along the x (b) and y axis (c). Experimental conditions: $[\text{BrO}_3^-]_0=65\text{ mM}$, $[\text{SO}_3^{2-}]_0=80\text{ mM}$, $[\text{Fe}(\text{CN})_6^{4-}]_0=20\text{ mM}$, $[\text{H}_2\text{SO}_4]_0=5.6\text{ mM}$ and $w=1.0\text{ mm}$.

acidic pulse moves from the left to the right. The space-time plot made along the x direction (Figure 3b) shows the characteristic of a relaxation oscillations. The period of oscillations

is about 17 min. It is important to notice, that the oscillatory phenomena is located to the inner part of the gel. On the space-time plot made along the y direction (Figure 3c) a slight phase shift can be noticed.

Numerical Simulations

In the experiments we can only follow the color change of the applied pH indicator, that provides information about the spatial pH distribution. The simulations serve the concentration distribution of all species in the CSTR and in the gel. In Figure 4 typical concentration profiles, which develop in the gel, are shown in the parameter domain of spatial bistability. Although, the CSTR is kept on the flow state, the concentrations at the CSTR/gel boundary ($x = 0$) differ from that of in the input feed. This demonstrate, that the input feed composition is only indirectly control the boundary composition at the CSTR/gel surface. At the F state (Figure 4a) the concentration of bromate and sulfite ions decreases smoothly along the x axis, but the concentration of hydrogen sulfite and ferrocyanide ions is almost constant in the gel. The ratio of $[\text{HSO}_3^-]/[\text{SO}_3^{2-}]$, which determines the local pH, changes from 0.282 at $x = 0$ mm to 2.34 at $x = 1.2$ mm.

At the M state (Figure 4b) a sharp stationary front, a sudden increase of the hydrogen ion develop in the middle of the gel. The sulfite ion concentration decreases almost linearly from the CSTR/gel surface to this point. In the acidic region of the gel both the hydrogen sulfite and ferrocyanide ion vanishes smoothly. The bromate ion profile is quite similar to that of the F state. Importantly, due to the presence of the hydrogen ion consuming pathway via reaction (R5-R7), the hydrogen ion concentration in the acidic core might be significantly lower than that of in the input feed. In case of the simulation presented in Figure 4 the input feed $[\text{H}^+]_0$ is 11.0 mM, while at the impermeable wall $[\text{H}^+](x = L_x)$ is only 0.54 mM.

In the parameter domain of bistability an appropriate acid perturbation, can induce a propagating front. The shape of the simulated (Figure 5) and the experimentally observed front (Figure 2) that connects the F and the M state are in good agreement. Both show a

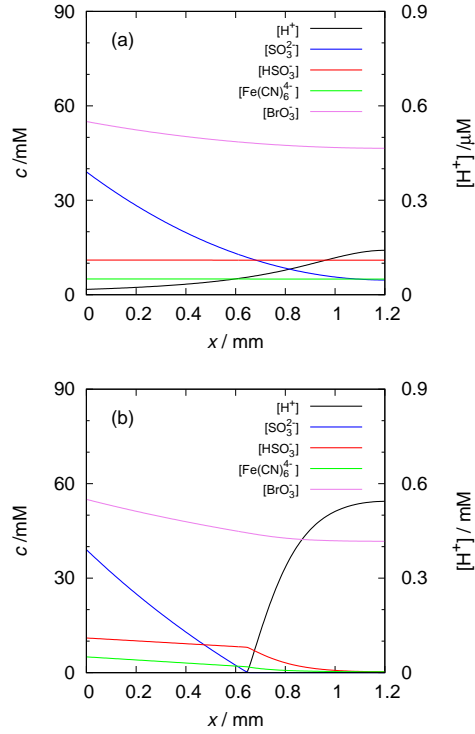


Figure 4: Simulated concentrations profiles at the F (a) and the M (b) states of the gel. The black, blue, red, green and violet line corresponds to the $[H^+]$, $[SO_3^{2-}]$, $[HSO_3^-]$, $[Fe(CN)_6^{4-}]$ and $[BrO_3^-]$ profile, respectively. The $[H^+]$ values are show on the the left y-coordinate. Parameters: $[BrO_3^-]_0=65$ mM, $[SO_3^{2-}]_0=80$ mM, $[Fe(CN)_6^{4-}]=5$ mM and $[H^+]_0=11.0$ mM, $w=1.2$ mm.

strong curvature in order to join up orthogonally with the impermeable wall. At the front

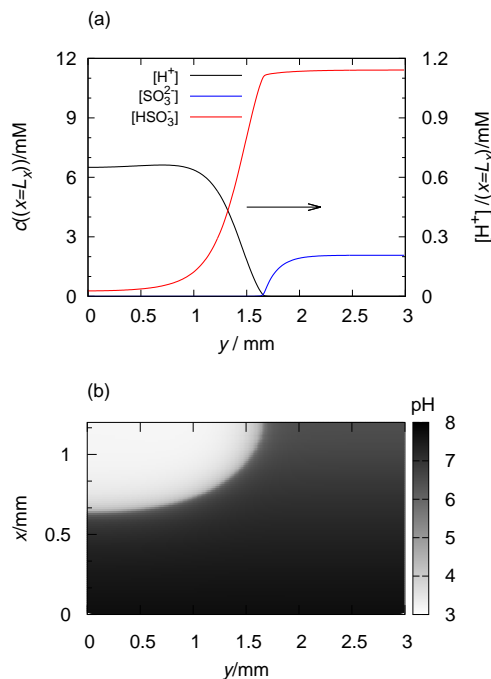


Figure 5: Simulated propagating front in the gel: concentration profiles along y at $x = L_x$ (a) and pH distribution along the x, y plane (b). The front propagates from the left to the right. The black, blue and red line corresponds to the $[H^+]$, $[SO_3^{2-}]$, $[HSO_3^-]$ profile, respectively. The $[H^+]$ values are shown on the the left y -coordinate. Parameters: $[BrO_3^-]_0=65$ mM, $[SO_3^{2-}]_0=80$ mM $[Fe(CN)_6^{4-}]_0=5$ mM and $[H^+]_0=11.5$ mM, $w=1.2$ mm.

position the sulfite ions are totally consumed and hydrogen ions are produced in expense of the hydrogen sulfite ions (Figure 5a). The hydrogen ion profile of the moving front shows a maximum, due to the presence of the hydrogen ion consuming reactions.

Above a critical $[Fe(CN)_6^{4-}]_0$ spatial bistability vanishes and spatiotemporal oscillation arises. At the experimental conditions used here and in our previously report,⁸ this limit is around 15 mM. The time-space plots made from the results of the numerical simulations (Figure 6) fit well to the experiments (Figure 3). The kinetic constants used in the simulations are valid at 25°C, while the experiments are made at 30°C. Taking into account, that the increase of temperature by 5°C shorten the period of oscillations by a factor of 1.5, the

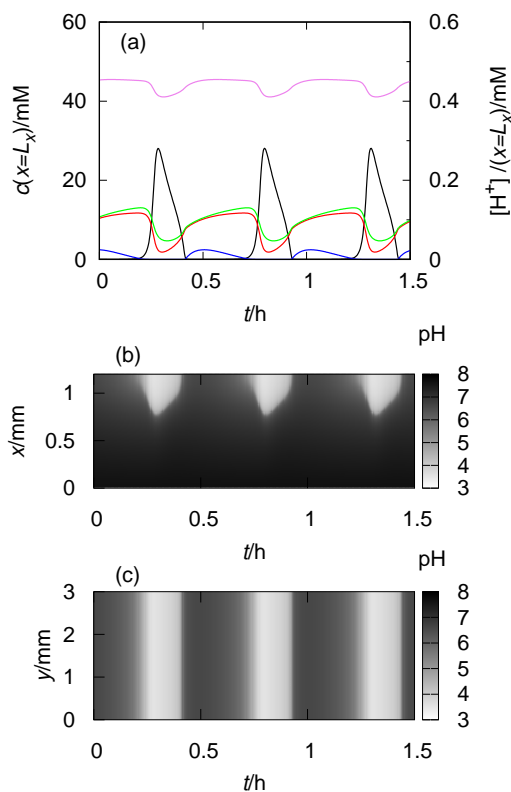


Figure 6: Simulated spatiotemporal oscillations in the gel at $x = L_x$ (a) and the corresponding time-space plots along the x (b) and y axis (c). The black, blue, red, green and violet line corresponds to the $[\text{H}^+]$, $[\text{SO}_3^{2-}]$, $[\text{HSO}_3^-]$, $[\text{Fe}(\text{CN})_6^{4-}]$ and $[\text{BrO}_3^-]$ profile, respectively. The $[\text{H}^+]$ values are on the the left y -coordinate. Parameters: $[\text{BrO}_3^-]_0 = 65 \text{ mM}$, $[\text{SO}_3^{2-}]_0 = 80 \text{ mM}$, $[\text{Fe}(\text{CN})_6^{4-}]_0 = 15 \text{ mM}$ and $[\text{H}^+]_0 = 12.2 \text{ mM}$, $w = 1.2 \text{ mm}$.

simulated and experimentally found periods are in good agreement. One important difference between the experimental observations and the simulation is, that in the simulations the oscillations develop homogeneously, without phase shift along the y axis. This can be caused by the relatively small extension of the reactor along the y axis in the simulations. Furthermore, the presence of inhomogeneities in the gel structure cannot be avoided in the experiments, and that can also results in the observed phase shift. The main lesson of the concentration *vs.* time curves (Figure 6a) is, that the hydrogen ion oscillates in antiphase with the sulfite, hydrogen-sulfite, ferrocyanide and bromate ions. Remarkably, the variation of the bromate ion concentration is small compare to its average value.

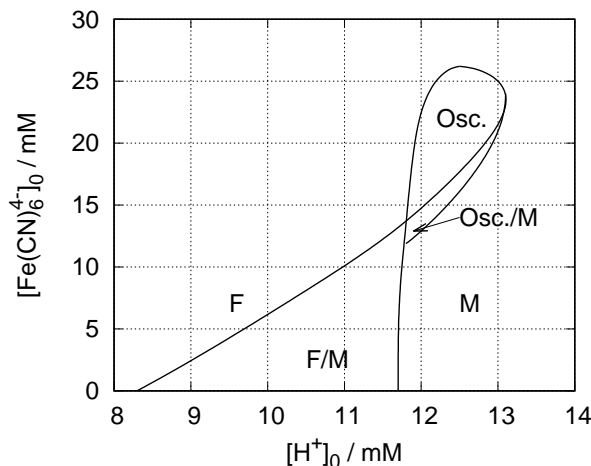


Figure 7: Simulated nonequilibrium phase diagram of the BSF reaction in OSFR along the $[H]_0$ - $[\text{Fe}(\text{CN})_6^{4-}]_0$ plane. The diagram shows the states of the gel, when the CSTR is maintained at the low extent of reaction stationary state. Parameters: $[\text{BrO}_3^-]_0=65 \text{ mM}$, $[\text{SO}_3^{2-}]_0=80 \text{ mM}$ and $w=1.2 \text{ mm}$.

The phase diagram along the $[H^+]_0$ - $[\text{Fe}(\text{CN})_6^{4-}]_0$ plane (Figure 7) shows the typical cross-shaped topology of the activator-inhibitor systems. In agreement with the experimental observations below a critical $[\text{Fe}(\text{CN})_6^{4-}]_0$ value only spatial bistability observed. A bifurcation diagram (Figure 8a), where the pH at $(x = L_x)$ are plotted against the control parameter $[H^+]_0$, represents this dynamics. At the actual conditions starting from $[H^+]_0 = 9 \text{ mM}$ the gel is on the F state, which is stable until $[H^+]_0 = 11.7 \text{ mM}$. Above this value only the M

state is stable. By decreasing $[H^+]_0$ the M state becomes unstable at $[H^+]_0 = 9.7$ mM.

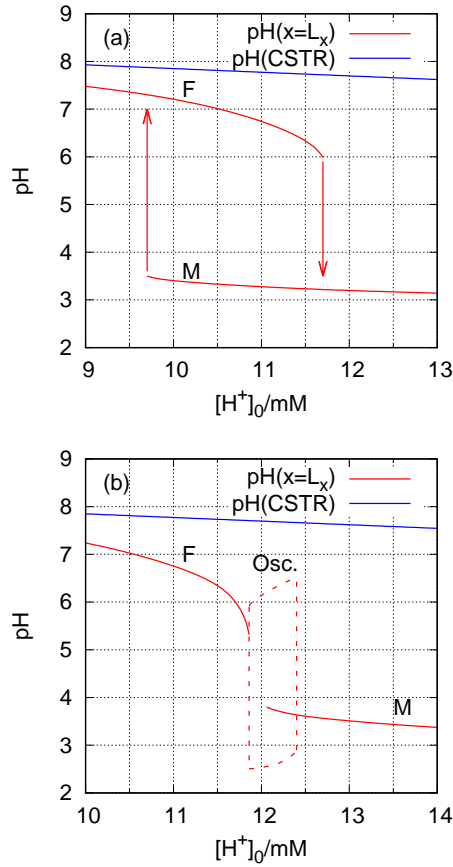


Figure 8: Simulated bifurcation diagrams at $[Fe(CN)_6^{4-}]_0 = 5$ mM (a), and at $[Fe(CN)_6^{4-}] = 15$ mM (b). The red line shows the pH in the gel at $(x = L_x)$ as a function of the control parameter $[H]_0$, while the blue line corresponds to the pH of the CSTR content. Parameters: $[BrO_3^-]_0 = 65$ mM, $[SO_3^{2-}]_0 = 80$ mM $w = 1.2$ mm.

The oscillations in the gel appear with a finite amplitude through a subcritical bifurcation (Figure 8b). Both stationary states overlap with the oscillatory one. The range of coexistence of the M and the oscillatory states is quite large. A similar dynamics have been found in the simulations made with a skeleton model of the mixed Landolt systems.²

Until this point we have only observed the appearance of the negative feedback in the presence of ferrocyanide. The expected effects of reaction (R5) and long range activation cannot be seen at the applied conditions. De Kepper and coworkers suggested, that the influence of the negative feedback in an OSFR depends on the thickness of the gel.² Simulations

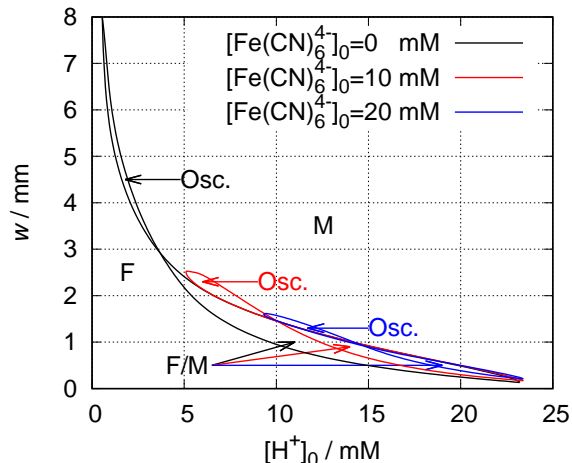


Figure 9: Simulated nonequilibrium phase diagram of the BSF reaction in OSFR along the $[\text{H}^+]_0$ - w plane at $[\text{Fe}(\text{CN})_6^{4-}]_0=0$ mM (black line), at $[\text{Fe}(\text{CN})_6^{4-}]_0=10$ mM (red line) and at $[\text{Fe}(\text{CN})_6^{4-}]_0=20$ mM (blue line). The diagram shows the states of the gel, when the CSTR is maintained at the low extent of reaction stationary state. Parameters: $[\text{BrO}_3^-]_0=65$ mM, $[\text{SO}_3^{2-}]_0=80$ mM.

are efficient to study this effect. The curves, that show the stability limits of the stationary states on the phase diagram along $[\text{H}^+]_0$ - w plane (Figure 9), follow the shape of reciprocal function. The important factors, which determine this shape, are the time scale of the diffusive feed and the induction time of the reaction between bromate and sulfite ions. As the first one is longer than the second one, the gel content stays on M state. The timescale of the diffusive feed (τ_f) scales with w^2 . For a chemical species with a diffusion coefficient D_i , at the core of the gel $x = L_x$ it can be calculated as $\tau_f = w^2/D_i$. The kinetic studies of the Landolt type reactions with different oxidants revealed, that the induction time, τ_i , scales with the reciprocal of the initial hydrogen ion concentration, e.g. $\tau_i \propto [\text{H}^+]_i^{-1}$.³⁴ Accordingly, in a thinner gel a higher value of $[\text{H}^+]_0$ is required to reach the M state.

In the absence of ferrocyanide the phase diagram shows spatial bistability below a critical value of $w = 3$ mm and oscillations above it. The appearance of oscillations in the gel is due to the presence of reaction (R5). If the rate constant of this reaction is arbitrary set to zero, the oscillation disappear. As ferrocyanide is added to the input flow, the critical value of w decreases and the domain of oscillation shifts to direction of lower thickness and higher

$[\text{H}^+]_0$. The effect of the two hydrogen ion consuming processes, reaction (R5) and reactions (R6-R7), cannot be separated. Since, the typical experiments are made in the range of $w = 3.0 - 0.75$ mm, we can conclude, that at these conditions the experimental observation of oscillations in the gel is not expected in the absence of ferrocyanide. However, at a large excess of bromate ions this dynamics have already been reported.²²

An important lesson of the phase diagrams in Figure 9 is, that the oscillatory/bistable dynamics appear between an upper and a lower critical limit of w . The upper limit of oscillations decreases with $[\text{Fe}(\text{CN})_6^{4-}]_0$. In the absence of ferrocyanide it is 8.0 mm and it goes to 1.6 mm at $[\text{Fe}(\text{CN})_6^{4-}]_0=20$ mM. The lower limit of bistability increases from 0.13 mm to 0.21 mm as $[\text{Fe}(\text{CN})_6^{4-}]_0$ is increased from zero to 20 mM.

The puzzling aspect of the phase diagram calculated in the absence of ferrocyanide (Figure 9 black line) is the lack of long range activation induced oscillation. On the base of the experimental result obtained in the IS reaction,²¹ we assumed, that this kind of dynamics might be favored at lower sulfite concentration. From the simulation made at different

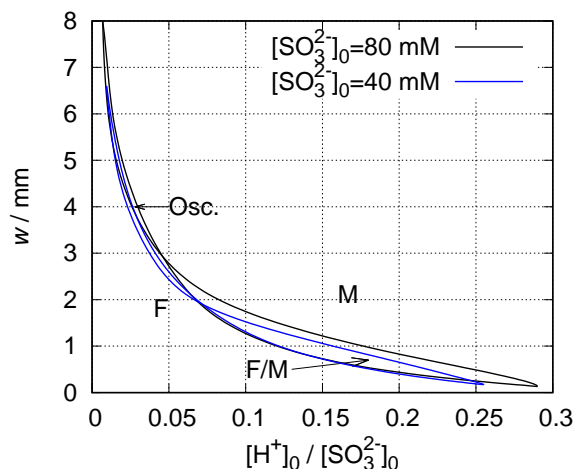


Figure 10: Simulated nonequilibrium phase diagram of the BS reaction in OSFR along the $[\text{H}^+]_0/[\text{SO}_3^{2-}]_0$ - w plane at $[\text{SO}_3^{2-}]_0=80$ mM (black line) and $[\text{SO}_3^{2-}]_0=40$ mM (blue line). The diagram shows the states of the gel, when the CSTR is maintained at the low extent of reaction stationary state. Parameters: $[\text{BrO}_3^-]_0=65$ mM, $[\text{Fe}(\text{CN})_6^{4-}]_0=0$ mM.

$[\text{SO}_3^{2-}]_0$, we have found out that the overall dynamics scales with $[\text{H}^+]_0/[\text{SO}_3^{2-}]_0$ ratio

(Figure 10). Low $[\text{H}^+]_0/[\text{SO}_3^{2-}]_0$ ratio (e.g. < 0.07) supports kinetic driven oscillations, while at high values of it bistability is preferred.

By fixing this ratio to 0.1, we have calculated a phase diagram along the $[\text{SO}_3^{2-}]_0-w$ plane (Figure 11a), where a small domain of spatiotemporal oscillations located at low values of $[\text{SO}_3^{2-}]_0$ appears. To clarify the origin of this periodic behavior, we arbitrary set to zero

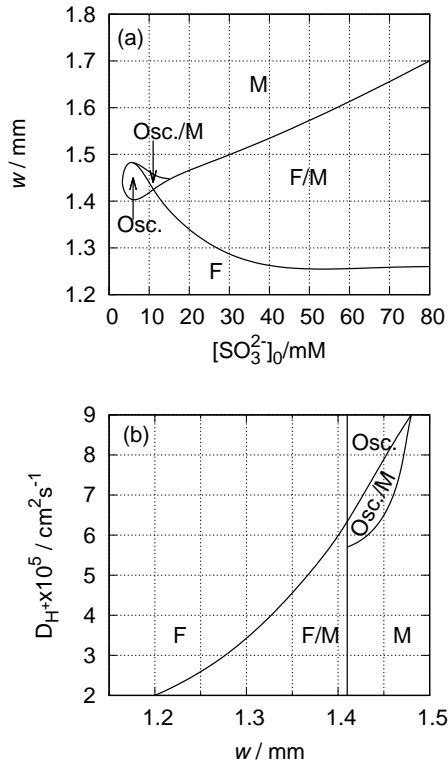


Figure 11: Simulated nonequilibrium phase diagram of the BS reaction in OSFR along the $[\text{SO}_3^{2-}]_0-w$ (a) and along the $w-D_{\text{H}^+}$ (b) plane. The diagram shows the states of the gel, when the CSTR is maintained at the low extent of reaction stationary state. Parameters: $[\text{BrO}_3^-]_0=65\text{ mM}$, $[\text{Fe}(\text{CN})_6^{4-}]_0=0\text{ mM}$, $[\text{H}^+]_0/[\text{SO}_3^{2-}]_0 = 0.1$ and in case of (b) $[\text{SO}_3^{2-}]_0=6\text{ mM}$, $[\text{H}^+]_0=0.6\text{ mM}$.

the rate constant of reaction (R5), but the oscillation does not disappear. Accordingly, the negative feedback, which drives the oscillatory dynamics at these conditions is not a kinetic instability. The phase diagram along the $w-D_{\text{H}^+}$ plane (Figure 11b) clearly shows, that these

oscillations are originated in long range activation. As the diffusion coefficient of hydrogen ion is arbitrary decreased the domain oscillations vanishes. Below, $D_{\text{H}^+} = 5.8 \times 10^{-5} \text{ cm}^2\text{s}^{-1}$ only bistability between the stationary F and M states are found. It is important to notice, that this long range activation driven oscillations develop only in tiny range of the thickness, that makes the experimental observation of this phenomena quite difficult.

Discussion

Some crucial parts of the experimentally observed versatile spatiotemporal dynamics of the BS/BSF reaction-diffusion system are accounted by a chemically realistic ten variable model. We have shown, that in an OSFR this mechanism is capable to produce spatiotemporal oscillations due to kinetic and also diffusion driven instabilities. The kinetic instabilities are linked to present of different hydrogen ion consuming steps, namely reaction (R5) and reactions (R6-R7). Although, the main antagonist of hydrogen ions are sulfite ions in this system, the development of oscillations require a process, which efficiently removes hydrogen ions at the acidic state of reaction, when sulfite ion cannot play this role. This is reaction (R5) in the absence and reaction (R6) and (R7) in the presence of ferrocyanide. These two kinetic pathways are linked to the same negative feed loop. The advantage of the presence of ferrocyanide is, that its input feed concentration is a convenient control parameter to find the conditions for the development of spatiotemporal oscillations.

The thickness of the gel (w) is a crucial parameter of the OSFR dynamics as it determines the value of the time scale of the diffusive feed at the innermost point of the gel. We have shown that the oscillatory/bistable dynamics appear between an upper and a lower critical limit of w . Interesting dynamical behavior cannot develop in a too thick or in a too thin gel. In an chemically inert and low density agarose gel, the effect of the gel matrix on the the diffusion of the components of the BSF reaction is negligible. A specific binding might appears for hydrogen ions due to the agaropectin residues, but previous measurements with

the same type of agarose gels do not find this effect to be significant. According to our simulations as $[\text{Fe}(\text{CN})_6^{4-}]_0$ increases the time scale of the negative feedback shortens and oscillations can develop in a thinner gel. The range of w at which oscillations can form is quite narrow. This sensitivity to thickness is in agreement with the experimental observations,⁸ and provides an explanation of the spatially localized nature of the oscillations recorded previously in a disc shape OSFR.⁸ Only a small spatial variation of the thickness of the gel, like a few tenth of a millimeter, can be enough to cause significant shift in the dynamics.

The simulations point out some interesting feature of the dynamics. The first is the reciprocal like relationship between the thickness of the gel and the hydrogen ion input feed concentration. In a thicker gel, lower hydrogen ion input feed concentration is required to switch from the F state to M and to get oscillations. The second lesson is the scaling of the dynamics according to $[\text{H}^+]_0/[\text{SO}_3^{2-}]_0$ ratio. Both seems a general feature of the Landolt type systems, and not specific to the BSF reaction. Although, the formation of oscillations due to long range activation is an expected result, but the small domain of oscillations found in the simulations, explains why this behavior have not been observed experimentally, yet.

Conclusions

Sustained reaction-diffusion patterns can only develop in open systems. The most popular tools for experimental study of these phenomena are the OSFR's, which are coupled dynamical systems. In an OSFR, a CSTR drives the dynamics of a gel part, which is a confined reaction-diffusion medium with mixed boundary conditions. The theoretical conditions for the development of spatiotemporal oscillations in a gel, which is fed from its boundary by a CSTR, are not known. However, a similar cross-shaped phase diagram topology found for the CSTR and for the gel in several different chemical systems, including the BSF reaction.^{4-6,8,35} The difficulties in the description of the dynamics often arise not only from the mathematical, but also from the chemical side. The BSF reaction is a prototype of the large

majority of oscillatory reactions, which oscillates only in the presence of continuous inflow of the reactants, because at least one of the initial reagents is nearly totally consumed during a period. Consequently, in the modeling of these systems pool chemical approximation is generally inappropriate. There are many other interesting phenomena observed in the BSF reaction-diffusion system, which are beyond the scope of this report. Calcium waves in the presence of calcium ions and ethylenediaminetetraacetate,⁷ or stationary patterns in the presence of sodium-polyacrylate,⁸ have also been reported. The ten variable model with the proper description of the coupled CSTR/gel system presented in this work, seems to provide a solid starting point to study all these complex dynamical behavior.

Acknowledgement

The authors thank the support of the National Research, Development and Innovation Fund (119360).

References

- (1) Orbán, M.; Kurin-Csörgei, K.; Epstein, I. R. pH-Regulated Chemical Oscillators. *Acc. Chem. Res.* **2015**, *48*, 593–601.
- (2) Szalai, I.; Horváth, J.; De Kepper, P. Contribution to an Effective Design Method for Stationary Reaction-Diffusion Patterns. *Chaos* **2015**, *25*, 064311.
- (3) Lee, K. J.; McCormick, W.; Ouyang, Q.; Swinney, H. Pattern-Formation by Interacting Chemical Fronts. *Science* **1993**, *261*, 192–194.
- (4) Horváth, J.; Szalai, I.; De Kepper, P. An Experimental Design Method Leading to Chemical Turing Patterns. *Science* **2009**, *324*, 772–775.
- (5) Szalai, I.; Horváth, J.; Takács, N.; De Kepper, P. Sustained Self-Organizing pH Patterns in Hydrogen Peroxide Driven Aqueous Redox Systems. *Phys. Chem. Chem. Phys.* **2011**, *13*, 20228–20234.
- (6) Liu, H.; Pojman, J. A.; Zhao, Y.; Pan, C.; Zheng, J.; Yuan, L.; Horváth, A. K.; Gao, Q. Pattern Formation in the Iodate-Sulfite-Thiosulfate Reaction-Diffusion System. *Phys. Chem. Chem. Phys.* **2012**, *14*, 131–137.
- (7) Molnár, I.; Kurin-Csörgei, K.; Orbán, M.; Szalai, I. Generation of Spatiotemporal Calcium Patterns by Coupling a pH-Oscillator to a Complexation Equilibrium. *Chem. Comm.* **2014**, *50*, 4158–4160.
- (8) Molnár, I.; Szalai, I. Pattern Formation in the Bromate–Sulfite–Ferrocyanide Reaction. *J. Phys. Chem. A* **2015**, *119*, 9954–9961.
- (9) Yoshida, R.; Ichijo, H.; Hakuta, T.; Yamaguchi, T. Self-Oscillating Swelling and Deswelling of Polymer Gels. *Macromol. Rapid Commun.* **1995**, *16*, 305–310.
- (10) Crook, C.; Smith, A.; Jones, R.; Ryan, A. Chemically Induced Oscillations in a pH-responsive Hydrogel. *Phys. Chem. Chem. Phys.* **2002**, *4*, 1367–1369.

- (11) Varga, I.; Szalai, I.; Mészáros, R.; Gilányi, T. Pulsating pH-Responsive Nanogels. *J. Phys. Chem. B* **2006**, *110*, 20297–20301, PMID: 17034210.
- (12) Horváth, J.; Szalai, I.; Boissonade, J.; De Kepper, P. Oscillatory Dynamics Induced in a Responsive Gel by a Non-oscillatory Chemical Reaction: Experimental Evidence. *Soft Matter* **2011**, *7*, 8462–8472.
- (13) Horvath, J. Peristaltic Waves in a Responsive Gel Sustained by a Halogen-Free Non-Oscillatory Chemical Reaction. *Polymer* **2015**, *79*, 243–254.
- (14) Rabai, G. Modeling and Designing of pH-Controlled Bistability, Oscillations, and Chaos in a Continuous-Flow Stirred Tank Reactor. *ACH - Models Chem.* **1998**, *135*, 381–392.
- (15) Benyaich, K.; Erneux, T.; Métens, S.; Villain, S.; Borckmans, P. Spatio-Temporal Behaviors of a Clock Reaction in an Open Gel Reactor. *Chaos* **2006**, *16*, 037109.
- (16) Borckmans, P.; Benyaich, K.; Dewel, G. Spatial Bistability: A Chemical Idiosyncrasy? *Int. J. Quant. Chem.* **2004**, *98*, 239–247.
- (17) Blanchedeau, P.; Boissonade, J. Resolving an Experimental Paradox in Open Spatial Reactors: The Role of Spatial Bistability. *Phys. Rev. Lett.* **1998**, *81*, 5007–5010.
- (18) Horváth, J.; Szalai, I.; De Kepper, P. Pattern Formation in the Thiourea-Iodate-Sulfite System: Spatial Bistability, Waves, and Stationary Patterns. *Physica D* **2010**, *239*, 776–784.
- (19) Boissonade, J.; Dulos, E.; Gauffre, F.; Kuperman, M. N.; De Kepper, P. Spatial Bistability and Waves in a Reaction with Acid Autocatalysis. *Faraday Discuss.* **2002**, *120*, 353–361.
- (20) Szalai, I. Spatiotemporal Behavior Induced by Differential Diffusion in Landolt Systems. *J. Phys. Chem. A* **2014**, *118*, 10699–10705.

- (21) Szalai, I.; De Kepper, P. Spatial Bistability, Oscillations and Excitability in the Landolt Reaction. *Phys. Chem. Chem. Phys.* **2006**, *8*, 1105–1110.
- (22) Virányi, Z.; Szalai, I.; Boissonade, J.; De Kepper, P. Sustained Spatiotemporal Patterns in the Bromate-Sulfite Reaction. *J. Phys. Chem. A* **2007**, *111*, 8090–8094.
- (23) Boissonade, J.; De Kepper, P. Multiple Types of Spatio-Temporal Oscillations Induced by Differential Diffusion in the Landolt Reaction. *Phys. Chem. Chem. Phys.* **2011**, *13*, 4132–4137.
- (24) Rábai, G.; Kaminaga, A.; Hanazaki, I. Mechanism of the Oscillatory Bromate Oxidation of Sulfite and Ferrocyanide in a CSTR. *J. Phys. Chem.* **1996**, *100*, 16441–16442.
- (25) Szántó, T. G.; Rábai, G. pH Oscillations in the BrO_3^- - SO_3^{2-} / HSO_3^- Reaction in a CSTR. *J. Phys. Chem. A* **2005**, *109*, 5398–5402.
- (26) Rabai, G.; Epstein, I. R. Systematic Design of Chemical Oscillators. 47. Kinetics and Mechanism of the Oxidation of Hexacyanoferrate (II) by Bromate. *Inorg. Chem.* **1989**, *28*, 732–736.
- (27) Kovacs, K.; Leda, M.; Vanag, V. K.; Epstein, I. R. Small-Amplitude and Mixed-Mode pH Oscillations in the Bromate- Sulfite- Ferrocyanide- Aluminum (III) System. *J. Phys-Chem. A* **2008**, *113*, 146–156.
- (28) Edblom, E. C.; Luo, Y.; Orban, M.; Kustin, K.; Epstein, I. R. Systematic Design of Chemical Oscillators. 45. Kinetics and Mechanism of the Oscillatory Bromate-Sulfite-Ferrocyanide Reaction. *J. Phys. Chem.* **1989**, *93*, 2722–2727.
- (29) Williamson, F. S.; King, E. L. The Kinetics of the Reaction of Sulfite and Bromate. *J. Am. Chem. Soc.* **1957**, *79*, 5397–5400.
- (30) De Kepper, P.; Boissonade, J.; Szalai, I. *Chemomechanical Instabilities in Responsive Materials*; Springer Netherlands, 2009; pp 1–37.

- (31) Hindmarsh, A. C.; Brown, P. N.; Grant, K. E.; Lee, S. L.; Serban, R.; Shumaker, D. E.; Woodward, C. S. SUNDIALS: Suite of Nonlinear and Differential/Algebraic Equation Solvers. *ACM T Math Software* **2005**, *31*, 363–396.
- (32) Lide, D. *CRC Handbook of Chemistry and Physics, 86th Edition*; Taylor & Francis, 2005.
- (33) Ouyang, Q.; Li, R.; Li, G.; Swinney, H. L. Dependence of Turing Pattern Wavelength on Diffusion Rate. *J. Chem. Phys.* **1995**, *102*, 2551–2555.
- (34) Molnár, I.; Takács, N.; Kurin-Csörgei, K.; Orbán, M.; Szalai, I. Some General Features in the Autocatalytic Reaction Between Sulfite Ion and Different Oxidants. *Int. J. Chem. Kinet.* **2013**, *45*, 462–468.
- (35) Szalai, I.; De Kepper, P. Pattern Formation in the Ferrocyanide-Iodate-Sulfite Reaction: The Control of Space Scale Separation. *Chaos* **2008**, *18*, 026105.

Graphical TOC Entry

